Fusion Engineering and Design 112 (2016) 621–627

Contents lists available at ScienceDirect

Fusion Engineering and Design

journal homepage: www.elsevier.com/locate/fusengdes

Lithium granule ablation and penetration during ELM pacing experiments at DIII-D

R. Lunsford[a,*], A. Bortolon[a], A.L. Roquemore[a], D.K. Mansfield[a], A. Nagy[a], R. Maingi[a], P.B. Parks[b], G. Jackson[b], E. Gilson[a], C.P. Chrobak[b]

[a] Princeton Plasma Physics Laboratory, Princeton, NJ 08543, USA
[b] General Atomics, San Diego, CA 92186-5608, USA

ARTICLE INFO

Article history:
Received 9 January 2016
Accepted 28 April 2016
Available online 25 May 2016

ABSTRACT

At DIII-D, lithium granules were radially injected into the plasma at the outer midplane to trigger and pace edge localized modes (ELMs). Granules ranging in size from 300 to 1000 microns were horizontally launched into H-mode discharges with velocities near 100 m/s, and granule to granule injection frequencies less than 500 Hz. While the smaller granules were only successful in triggering ELMs approximately 20% of the time, the larger granules regularly demonstrated ELM triggering efficiencies of greater than 80%. A fast visible camera looking along the axis of injection observed the ablation of the lithium granules. The duration of ablation was used as a benchmark for a neutral gas shielding calculation, and approximated the ablation rate and mass deposition location for the various size granules, using measured edge plasma profiles as inputs. This calculation suggests that the low triggering efficiency of the smaller granules is due to the inability of these granules to traverse the steep edge pressure gradient region and reach the top of the pedestal prior to full ablation.

Published by Elsevier B.V.

1. Introduction

Periodic expulsions of energy and particles, termed Edge Localized Modes (ELMs), are often a consequence of operating a toroidal plasma device in high confinement or "H-Mode". As the energy stored within the discharge increases in future burning plasma devices such as ITER, the unmitigated transient power flux arriving at the divertor and wall during an ELM is projected [1] to be substantially above the damage threshold of current plasma facing component (PFC) designs. One of the baseline strategies for mitigating this heat flux is to rapidly pace the ELMs above their natural frequency so that the amount of energy exhausted to the PFCs is reduced inversely with the triggering frequency [2,3]. This augmentation of the natural ELM frequency can be accomplished by repeated injection of non-fueling impurity granules from the low field side of the discharge. The ablation of these granules in the edge plasma is hypothesized [4] to lead to the creation of high density filaments which generate 3-D pressure gradients that destabilize ballooning modes and manifest as ELMs.

At DIII-D, lithium granules ranging in size from 300 to 900 μm in diameter were injected into various discharges with low natural ELM frequencies to test this principle [5]. A vibrating piezoelectric disk gravitationally fed a rotating impeller which drove granules into the edge plasma at velocities ranging from 50 to 150 m/s. This resulted in an increase in the nominal ELM frequency for these discharges from its natural 10–15 Hz to 30–100 Hz, with a corresponding reduction of the peak heat flux as measured by IR thermography at the divertor strike points. The increased ELM frequency and the corresponding particle outflux were also observed to clamp the rise of nickel impurity buildup within the core.

Utilizing high speed imaging along the granule insertion trajectory, we have recorded the expansion of the ablation cloud and measured ablation times of several hundred μs. The duration of the granule ablation event is then used to benchmark a neutral gas shielding (NGS) model [6] of pellet injection, from which a granule penetration depth can be inferred. The remainder of this paper is organized as follows: Section 2 describes the injector and diagnostics, Section 3 summarizes the ELM pacing experiments, Section 4 describes the NGS model, and Section 5 presents ablation results as a function of granule size and velocity.

* Corresponding author.
E-mail address: rlunsfor@pppl.gov (R. Lunsford).

http://dx.doi.org/10.1016/j.fusengdes.2016.04.041
0920-3796/Published by Elsevier B.V.

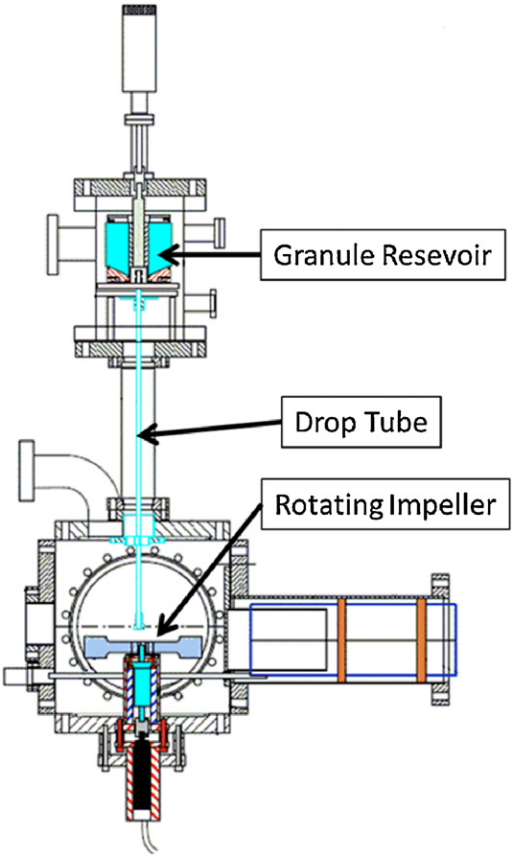

Fig. 1. Assembly drawing of the lithium Granule Injector (LGI) showing the principal working components.

2. Lithium granule injector

The Lithium Granule Injector (LGI) used for these experiments extends a previously demonstrated concept for the application of lithium powder into the edge of fusion plasmas [7,8]. The design of the powder dropper has been adapted to allow the horizontal injection of solid impurity granules into the edge of fusion research plasmas. A cutaway of the granule injector is shown in Fig. 1, and described in more detail in reference [9]. While the injector has been tested on several different types of impurity granules, the experiments discussed herein are confined to the injection of lithium granules, due to the low atomic number of lithium and the documented beneficial effects of the application of lithium doses in high confinement discharges [10,11].

2.1. Experimental apparatus

The granules to be injected are stored in a segmented chamber which allows the manual selection between 4 different sizes of granules. Lithium granules are presorted and subdivided into four batches with diameters ranging from 200 to 400, 400–600, 600–800, and 800–1000 μm. Each batch is then placed into its own chamber within the granule reservoir called out in Fig. 1, while the granule injector is held within an inert argon atmosphere. This precaution is required to keep the lithium granules from reacting with the atmosphere and forming a lithium oxide coating which would bind the granules together. Selection of the desired granule chamber is performed by the rotation of a central shaft. The shaft has a single opening milled into a section of the lower extent of the shaft which acts as a door. The door opens a specific quadrant of the dropper housing allowing granules to fall onto a piezoelectric disk immediately below the granule chamber.

The piezoelectric disk is driven at resonance which pushes the granules toward a central opening. This hole at the center of the disk is directly above a drop tube which allows the granules to be gravitationally accelerated down the guide tube where they are driven into the plasma by a rapidly rotating pneumatically driven impeller. The LGI has been tested on granules ranging in size from 300 to 900 microns at injection velocities from 50 to 150 m/s and with granule injection frequencies of up to 500 Hz as determined by the rotation frequency of the impeller.

Note that the impeller and the vibrating piezoelectric disk are not coupled either electrically or mechanically, resulting in asynchronous delivery of granules into the edge of the discharge. Therefore the injection frequency does not exhibit a regular periodicity, but rather a variable frequency determined by the reciprocal of the granule to granule period.

2.2. Diagnostic capabilities

The LGI has a set of dedicated diagnostics which monitor the operation of the granule injector as well as the ablation of the injected granules. The impeller chamber is illuminated by a pair of high intensity halogen lamps, and the location where the falling granules meet the impeller is recorded by a Phantom 7.3 high speed camera. The images of the granule impact with the impeller are recorded at 20 kHz; automated analysis is used to determine the injection frequencies and injection times. A photodiode attached to the rear of the impeller cube is utilized for a rapid real-time measurement of the impeller rotation frequency. In addition, a second high speed camera is mounted on the rear of the impeller cube and its field of view is directed radially inward. This camera is utilized to monitor the illumination resulting from the ablation and rapid ionization of the granule material. Respective images (Fig. 2) from the ablation of a 400, 600, and 800 μm granule display behavior consistent with the ablation model presented in Fig. 5 and discussed in Section 4. The 400 μm granule ablation was recorded on DIII-D discharge #160406 at t = 1.60135 s and the 600 and 800 μm granules represent the lower and upper bounds of the granule sizes utilized in DIII-D 160416 and can be found at t = 2.1176 and t = 1.8179 s respectively. The granule diameters are determined from the initial ablation frame for each respective granule injection event, in which the granule itself is unobscured by the ablation cloud. Once the granule begins to ablate the color images show the field aligned ablation cloud whose emission is primarily due to the singly ionized lithium transition at 548 nm. Each frame is separated by 50 μs, allowing the duration of the ablation event to be approximated by the number of illuminated frames.

3. Lithium granule injection experiments

The lithium granule pacing experiments described herein were performed at the DIII-D National Fusion Facility [5]. The reference discharge into which the granules were injected were deuterium plasmas in a lower single null divertor configuration. The plasma was developed with an ITER-like shape, a plasma current (I_P) of 1.2 MA, a toroidal field B_T of 2.0 T, a normalized pressure $\beta_N = 1.5$, and a safety factor (q_{95}) of approximately 4.6. With a neutral beam heating power of 4 MW, these H-mode discharges have a natural Type I ELM frequency of approximately 12 Hz, represented by the black traces in Fig. 3, this is compared with a discharge where granules were used to pace ELMs (red traces).

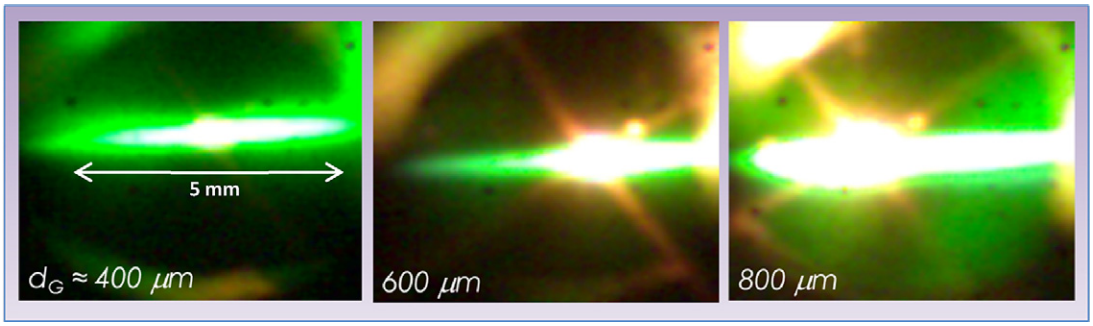

Fig. 2. Ablation of lithium granules as captured by the LGI camera. These three images, taken from two different discharges demonstrate the differences in ablation intensity for three different size granules. The granules are injected radially inward, which in these images is directed into the page. The ablation cloud spreads laterally from the granule core, aligned with the local magnetic field geometry. The crosses seen in the 600 and 800 μm images and aligned with the granule core are due to lens flares caused by the brightness of the ablation event.

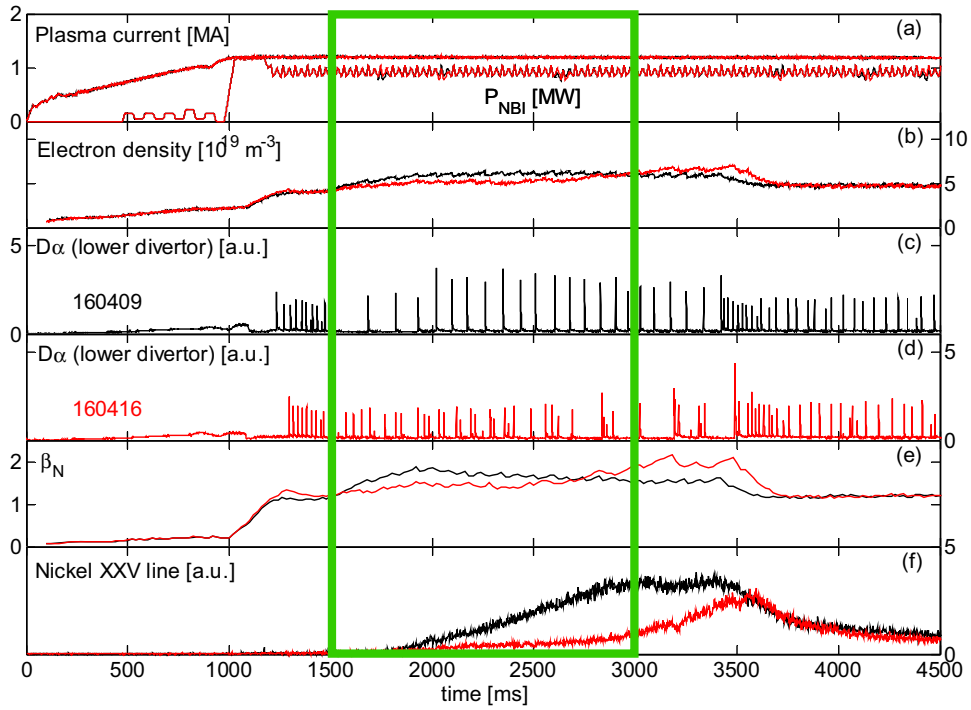

Fig. 3. Plasma parameters for both a baseline (160409 : black) and LGI paced (160416 : red) discharge. The green box is indicative of the period of the discharge where reliable lithium granule injection was observed. (For interpretation of the references to colour in this figure legend, the reader is referred to the web version of this article.)

3.1. Elm triggering by granule injection

An examination of pellet injection effect and the corresponding ELM triggering physics has been performed with the non-linear MHD code JOREK [4]. It indicates that as the pellet or granule enters the discharge there is an adiabatic expansion of the ablatant cloud which travels along the relevant field lines at an ion thermal speed, with typical timescales of approximately 200 μs. In response to this cold high density region, a rapid electron conduction thermalizes the cloud with timescales of 5 μs. Thus the heat flows in faster than the density can flow out of the deposition region. This leads to a polodially and torodially localized increase in the plasma pressure which, if localized near the top of the pedestal, will add to the pre-existing gradient, thus leading to the destabilization of high-n ballooning modes resulting in an ELM crash event. Given sufficient pedestal rebuilding time between the injection events, additional granule injections can then be used to drive further ELMs resulting in pacing.

Deuterium pellet injection experiments have demonstrated [3,12,13] that the energy release and peak heat flux from an ELM is inversely proportional to the ELM frequency. Experiments performed on ASDEX-U, JET-C (Carbon Wall), and DIII-D have shown that rapid pacing of ELMs with continuous injection of small pellets from the low field side does reduce the peak heat flux and is compatible with the High Field Side fueling requirements. Thus rapidly triggering ELMs to reduce the peak heat flux to a level tractable for the PFCs is presently a baseline mitigation technique for ITER [2]. However, recent results from JET-ILW [14] (ITER-Like-Wall), and AUG-W [15] (ASDEX-U with tungsten walls) have suggested that the change in wall composition has led to a modification of the pellet-ELM triggering event. This has manifested as a diminished reciprocal behavior of the peak heat flux and a reduced pacing effect. There is also the observed appearance of an “ELM trigger lag time”, a post-ELM duration wherein it is not possible to trigger a subsequent ELM with the available pellet sizes. The existence of such a phenomenon suggests that there is an upper frequency limit for this pacing technique.

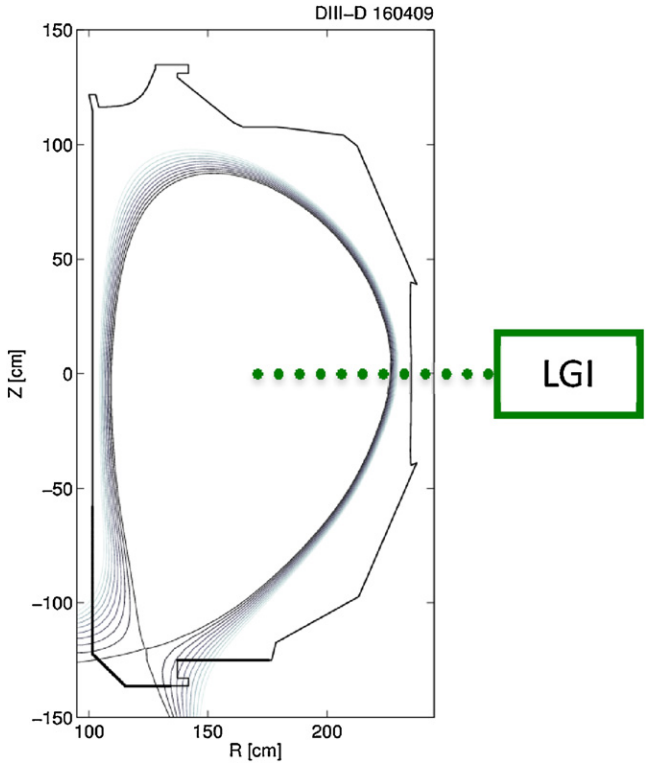

Fig. 4. Shape of the LGI injected plasma and injection geometry for the lithium granules.

Like deuterium pellet pacing, the triggering of ELMs by granule injection is dependent upon both the granule size and the pedestal edge parameters. If the pedestal pressure has rebuilt during the inter-ELM period to a level near that required for destabilization of an ELM, then even a small perturbation might be successful in instigating an ELM crash event. By the same token, granules of a sufficient size should be capable of destabilizing ELMs at any point during pedestal recovery within the natural inter-ELM evolution. Using impurity granules to pace ELMs decouples the pacing function from the concomitant fueling which results from deuterium pellet pacing, possibly allowing greater flexibility in the choice of granule size required to pace ELMs at a given frequency. On the other hand, impurity granules might lead to an increase of Z_{eff}, and possibly dust production via chemical reactions, which would need vigilant monitoring.

3.2. Results of granule injection

Lithium granules of varying sizes were injected into H-mode discharges at a range of injection velocities and granule-to-granule frequencies as described in Section 2.1. As shown in Fig. 4, the LGI was located at the nominal discharge midplane, with granules injected in an essentially horizontal direction. As expected, the injected granules ablated as they entered the edge of the discharge, creating a field aligned high density filament shown as the saturated horizontal regions in Fig. 2. For granules below 500 μm, the injection was successful in triggering an ELM approximately 30% of the time. In the cases where the perturbation seeded by these granules was insufficient to generate an instability, the resulting density input was then equilibrated throughout the discharge. The triggering efficiency increased sharply with granule size. In experiments where the granule sizes were larger than 700 μm the triggering efficiency was greater than 80%, approaching 100% in some discharges.

Table 1
Mass deposition located past the pedestal shoulder for a range of injection sizes and velocities.

Granule Size	Granule Velocity	Atoms deposited atop the pedestal
400 μm	50 m/s	3.68×10^{16}
400 μm	100 m/s	4.11×10^{17}
600 μm	50 m/s	7.54×10^{17}
600 μm	75 m/s	1.66×10^{18}
600 μm	100 m/s	2.31×10^{18}
600 μm	125 m/s	2.77×10^{18}
800 μm	50 m/s	3.29×10^{18}
800 μm	100 m/s	6.85×10^{18}

For all granule sizes, these triggering efficiencies were only weakly correlated to injection frequency and granule velocity.

The LGI has been used for full ELM pacing at augmented ELM frequencies of 3 times the natural discharge frequency for ~5 s discharge without confinement degradation. The paced ELM frequency was increased from 12 to 38 Hz for the full discharge and was increased transiently up to 100 Hz in other discharges. While this elevated pacing reduced the overall energy confinement by up to 10%, the normalized confinement relative to the ITER $H_{98,Y2}$ scaling remained constant. In addition the rapid pacing of ELMs by granule injection was observed to reduce the level of core carbon impurity concentration as well as clamping the accumulation of higher Z metallic impurities. As a result, even though the largest granules penetrated deeply, the core volume averaged Z_{eff} did not increase due to the lithium injections, and in some instances Z_{eff} was observed to decrease by ~15% due to the pacing efforts.

4. Ablation simulation with neutral gas shielding model

To characterize the ablation of the lithium granules as they enter the edge plasma, we utilized the NGS or Neutral Gas Shielding model [6]. In this model, high energy electrons impact the incoming granule and create a cloud of neutral lithium which surrounds the remaining granule (Fig. 5). Heat transfer from the background plasma then ionizes the ablated lithium, which streams out along the field lines. The surrounding neutral gas cloud subsequently mediates the flow of energy to the solid granule; as long as sufficient mass remains in the granule to sustain the cloud, this shielding will be maintained. However, once the granule is fully ablated, the cloud dissipates and the local lithium density quickly equilibrates on a timescale less than 50 μs.

As mentioned previously, the camera which captures these images is located behind the LGI system and maintains a view directed radially into the plasma, collinear with the direction of injection. The overall cigar shape of the ablating granule can be seen in the captured images and is indicative of the granule itself being obscured by the high density neutral core and the field aligned ionization cloud. This is consistent with previous observations [16,17] of granule injection and ablation as benchmarked against the NGS model [18,19]. The ablation rate (**G**) of the injected granules is given by Equation (1).

$$G = \frac{4\pi r_g^2 q_s \eta f_B}{n_g}\left[\Delta H + \frac{10}{3}T_s\right]^{-1} \quad (1)$$

where r_g and n_g are the radius and density of granule respectively, η is the cloud shielding parameter, f_B is the product of the field directed anisotropy and flux screening parameter, with a value of 0.08 [14], ΔH is the sublimation energy of lithium (1.6 eV/atom), and T_S is the surface temperature of the granule, which was taken as the boiling point of lithium (0.14 eV). The plasma parameters

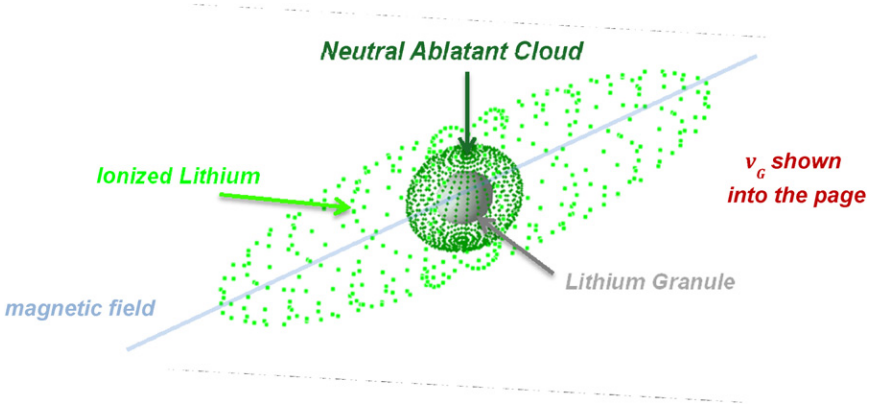

Fig. 5. Illustration of the components of the granule ablation. As the granule enters the plasma, here shown with a velocity directed into the plasma, electron conduction ablates the surface and creates a dense neutral cloud around the granule. Further heat conduction ionizes the neutral cloud which streams out along the magnetic field lines.

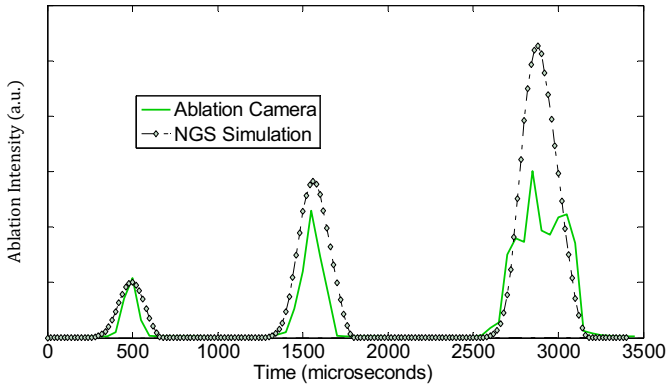

Fig. 6. Ablation Camera record and NGS simulation. The solid green line shows the integrated ablation intensity recorded for the three granule sizes shown in Fig. 2. The dotted line shows the corresponding NGS simulation with a cloud shielding parameter of 0.3. Intensities are normalized to the smallest granule size. (For interpretation of the references to colour in this figure legend, the reader is referred to the web version of this article.)

are subsumed within the heat flux variable q_S which is given by Equation (2).

$$q_s = \frac{1}{2} n_e T_e \left(\frac{8T_e}{\pi m_e} \right)^{1/2} \tag{2}$$

As we do not know a priori the cloud shielding efficiency of the neutral lithium cloud, we have used this as a fit parameter for the model. The ablation traces shown in Fig. 6 are the integrated time histories of the ablation events described in Section 2.2 and shown in Fig. 2, transferred to a single x-axis for ease of comparison (i.e. the three ablation events are from different discharges, not closely spaced in a single discharge). The integrated detector intensity for the 400 μm granule ablation event is plotted first, followed by the 600 and 800 μm granules, as the single solid green curve. We adjusted the shielding efficiency parameter such that the time envelope of the ablation calculation (dotted line) matched the observed ablation duration for the largest granule. These calculated ablation amounts are then normalized so that the peak ablation of the 400 μm granule simulation is equivalent to the observed maximum intensity of the smallest granule. Fig. 6 shows that the NGS predictions are reasonably effective at reproducing the ablation profile. There is an underestimation of the intensity as the granule size increases, this is likely due to a saturation of the detector, which becomes more pronounced as the intensity increases.

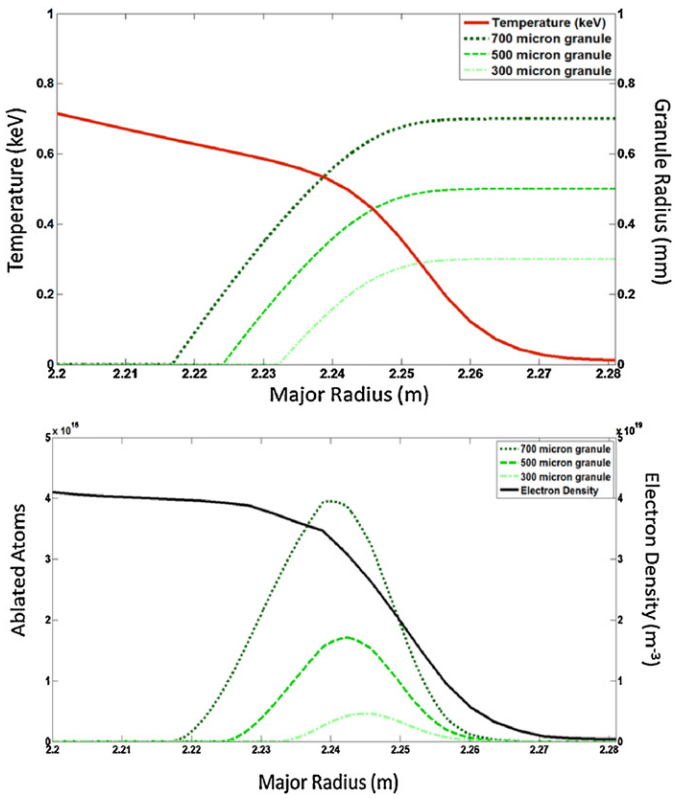

Fig. 7. Radial decay and ablation deposition calculation for simulated granules. The upper panel displays the decay of the granule diameter for 700, 500, and 300 μm granules, while the lower panel displays the deposition location of the ablated atoms with respect to the density pedestal.

5. Granule ablation and mass deposition

Having calibrated the NGS model by fitting the ablation time envelope to the experimental observations, it can then be used to calculate the rate of radial decay which specifies the granule penetration depth as it enters the edge of the plasma. Fig. 7 shows this result for three different granule sizes. The penetration depths were found to range from 2 to 5 cm depending upon the size of the injected granule. This data then allows an estimation of the mass deposition location with respect to the plasma density profile in the steep gradient region. As shown in the upper panel, the granule diameter decays rapidly as the injected material enters the edge plasma. This results in a peak mass deposition primarily located in

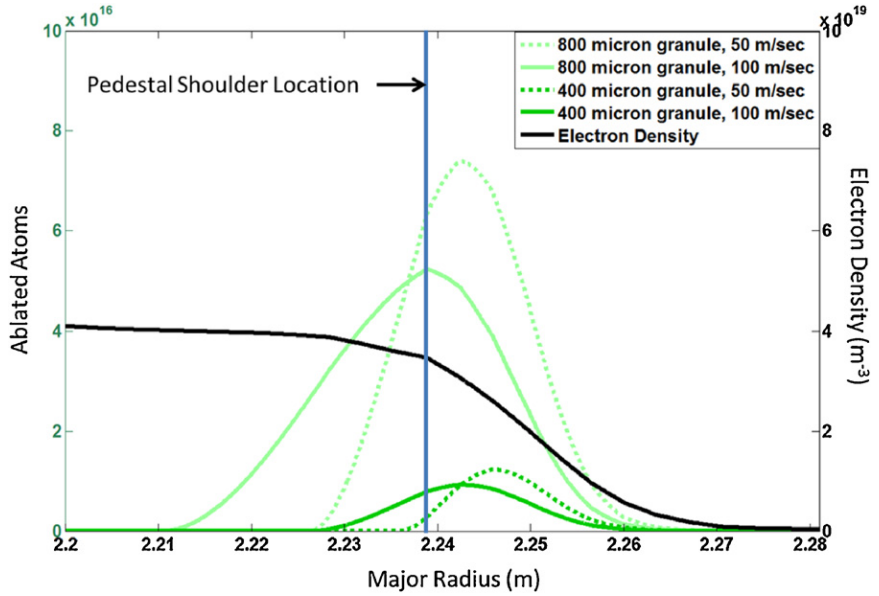

Fig. 8. Ablation deposition for large and small granules at high and low velocities. The vertical line denotes the shoulder of the pedestal.

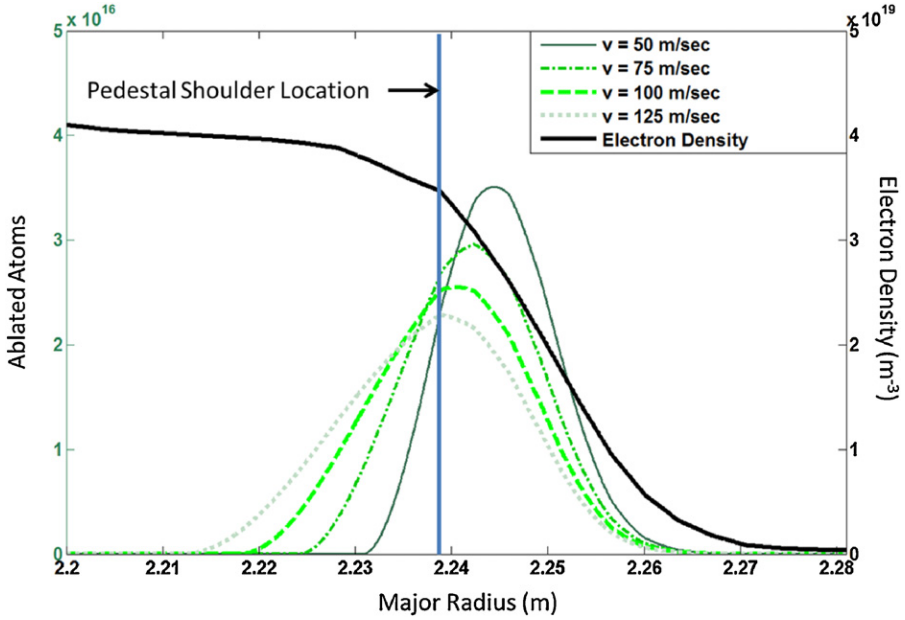

Fig. 9. Deposition of ablatant material for 600 μm granule at a range of injection velocities. The vertical blue line represents the shoulder of the pedestal. (For interpretation of the references to colour in this figure legend, the reader is referred to the web version of this article.)

the steep gradient region (lower panel). Thus, while some portion of the injected granule does penetrate deeply into the edge plasma, the majority of the mass is distributed much closer to the separatrix.

This deposition profile indicates why the granule triggering efficiency is primarily dependent upon the size of the granule and is largely insensitive to variations in the granule injection velocity over the ranges accessible to the LGI [5]. As is shown in Fig. 8, a pair of simulated 400 μm granules are injected at 50 and 100 m/s, near the upper and lower mechanical limits of the injector. Both granules are found to ablate rapidly upon entering the edge of the discharge, independent of the injection velocity. Note that only a small portion of the ablated mass is deposited at the top of the pedestal, i.e. the depth at which ELM triggering efficiency theoretically increases. In contrast, while there is substantial ablation of the 800 μm granules in the steep gradient region, there is still a substantial amount of mass deposited near the top of the pedestal, independent of the injection velocity of the granule. Note that velocities below 40 m/s are impractical for horizontal injection, due to gravitational acceleration and downward drift. Also, these calculations assume a constant velocity for the granule and do not take into account any deceleration effects which have been noted with deuterium pellets. Were such an effect present, it would shift the mass deposition profile further outward, an outcome that will be explored further in future experiments.

Given that the 400 μm granules trigger ELMs irregularly while the 800 μm granules trigger them on a more consistent basis, we postulate that there should be an intermediate granule size where there is a more discernable dependence between injection velocity

and triggering efficiency. To explore this, Fig. 9 displays the simulated injection of 600 μm granules at a range of injection velocities, a parameter set we were unable to access during the experiment due to a limited quantity of this granule size. By integrating the number of atoms deposited past the pedestal shoulder, we can see that an intermediate size granule at a range of attainable velocities will span the mass deposition gap between the large and small granules, as summarized in Table 1. This should provide insight to the mass dependence threshold and relevant triggering mechanism leading to a determination of the minimal granule perturbation required for reliable ELM triggering.

6. Summary

By increasing the frequency of the ELMs through the injection of sub-millimeter sized lithium granules, the LGI has demonstrated the ability to fully pace ELMs in multi-second discharges. This pacing has lead to the reduction of the observed peak heat flux and a clamping of the high-Z metal impurities [5]. The granule injection has been observed by a radially viewing ablation camera, which has noted an ablation behavior consistent with previous pellet injection observations [16–19]. We have implemented a NGS model for lithium, extending the previous model simulations used for deuterium pellets. The granule shielding free parameters in the model were calibrated by comparison with the time envelope of the ablation data for several granule sizes. The model was subsequently used to compute the ablation rates and radial deposition profiles. It was observed that the smallest granules, which had a low triggering probability, deposited small amounts of mass near the top of the pedestal. The largest granules, on the other hand, deposited substantial amounts of mass in the pedestal, consistent with their high ELM triggering probability. While neither of these granule sizes was sensitive to the radial granule velocity, calculations showed that an intermediate granule size should exhibit more sensitivity than the ones that were tested. This motivates future experiments on the impact of granule velocity on ELM triggering probability at intermediate size, while also confirming the utility of the largest granules for effective ELM pace-making. Looking forward, these types of experiments will be repeated with other impurities such as carbon and boron, which will allow a further test and extension of the NGS model, with the prospect of predicting the necessary conditions for ELM pacing with impurity granules in future devices like ITER.

Acknowledgment

Supported in part by the U.S. Dept. of Energy under contracts DE-AC02-09CH11466[1] and DE-FC02-04ER54698[2]. DIII-D data shown in this paper can be obtained in digital format by following the links at https://fusion.gat.com/global/D3D_DMP.

References

[1] T.E. Evans, ELM mitigation techniques, J. Nucl. Mater. 438 (2013) S11–S18.
[2] A. Loarte, et al., Progress on the application of ELM control schemes to ITER scenarios from the non-active phase to DT operation, Nucl. Fusion 54 (2014) 033007.
[3] L.R. Baylor, et al., Reduction of edge-localized mode intensity using high-repetition-rate pellet injection in tokamak H-mode plasmas, Phys. Rev. Lett. 110 (2013) 245001.
[4] S. Futatani et, al.: Non-linear MHD modelling of ELM triggering by pellet injetgion in DIII-D and implications for ITER, Nucl. Fusion 54 (2014) 073008.
[5] A. Bortolon, et al., High frequency pacing of edge localized modes by injection of lithium granules in DIII-D H-mode discharges, Nucl. Fusion (2016), NF-100993.
[6] P. Parks, et al., Analysis of low Z_a impurity pellet ablation for fusion diagnostic studies, Nucl. Fusion 28 (1988) 477.
[7] D.K. Mansfield, et al., A simple apparatus for the injection of lithium aerosol into the scrape-off layer of fusion research devices, Fusion Eng. Design 85 (2010) 890.
[8] A.L. Roquemore, et al., Techniques for injection of pre-characterized dust into the scrape-off layer of fusion plasma, Fusion Eng. Design 86 (2011) 1355.
[9] D.K. Mansfield, et al., First observations of ELM triggering by injected lithium granules on EAST, Nucl. Fusion 53 (2013) 113023.
[10] R. Maingi, et al., Dependence of recycling and edge profiles on lithium evaporation in high triangularity: high performance NSTX H-mode discharges, J. Nucl. Mater. 463 (2015) 1134–1137.
[11] T.H. Osborne, et al., Enhanced H-mode pedestals with lithium injection in DIII-D, Nucl. Fusion 55 (2015) 063018.
[12] L.R. Baylor, et al., Reduction of edge localized mode intensity on DIII-D by on-demand triggering with high frequency pellet injection and implications for ITER, Phys. Plasmas 20 (2013) 082513.
[13] A.W. Leonard, Edge-localized-modes in tokamaks, Phys. Plasmas 21 (2014) 090501.
[14] P.T. Lang, et al., ELM pacing and trigger investigations at JET with the new ITER-like wall, Nucl. Fusion 53 (2013) 073010.
[15] P.T. Lang, et al., ELM pacing and high-density operation using pellet injection in the ASDEX Upgrade all-metal-wall tokamak, Nucl. Fusion 54 (2014) 083009.
[16] H.W. Müller, et al., High β plasmoid formation, drift and striations during pellet ablation in ASDEX upgrade, Nucl. Fusion 42 (2002) 301.
[17] V.A. Rozhansky, I. Yu, Senichenkov On the Ablation Models of Fuel Pellets, Plasma Phys. Rep. 31 (12) (2005) 993.
[18] P.B. Parks, et al., Model of ablation flow near light-atom pellets with surface boundary conditions, Nucl. Fusion 34 (3) (1994) 417.
[19] G. Kocsis, et al., On the fluctuation of line radiation emitted during aluminum micro-pellet ablation in magnetized plasmas, PPCF 41 (1999) 881–898.